

Spline Surface Fitting using Normal Data and Norm-like Functions

Agnes Seiler¹, David Großmann², and Bert Jüttler³

¹*DK Computational Mathematics, Johannes Kepler University, Linz/Austria,
agnes.seiler@dk-compmath.jku.at*

²*MTU Aero Engines AG, Munich/Germany*

³*Institute of Applied Geometry, Johannes Kepler University, Linz/Austria*

Abstract

This paper is motivated by the geometry reconstruction process for aircraft engines. In order to improve the overall smoothness of the resulting spline surface, we consider the simultaneous approximation of point and normal data. If the normal data to be approximated by one patch is taken from the boundary of its neighbors, this controls the behavior of the resulting spline patch along the boundary and ensures approximate G^1 -smoothness of the composite surface. We show that for every mesh size there exists a solution to the resulting optimization problem. Optimal convergence is achieved based on an appropriate choice of the weight controlling the relative influence of points and normals, taking the distinct approximation order of splines for points and derivatives into account. In addition we investigate the effect of using norm-like functions for measuring the errors.

1 Introduction

Spline surface fitting is a well-established technique for surface reconstruction from point data (Hansford and Farin, 2002; Dierckx, 1995). It is frequently used in industrial applications, where the scanning of mechanical components results in point cloud data. For subsequent processes it is often necessary to find a surface that represents the point data. Typically, the triangulated data sets are segmented and the resulting pieces are parameterized and fitted individually. After the fitting step, the collection of the approximating patches forms the geometric model that is now suitable for further processing.

The importance of fitting in an industrial context, i.e., as a part of the so-called reverse engineering (Varady, 1997), is evident from the substantial number of publications on this topic. Besides algebraic and implicit surfaces (Jüttler and Felis, 2002) as well as subdivision surfaces (see Ma, 2005; Marinov and Kobbelt, 2005), which appear to be not fully supported by all existing software tools (Shi et al., 2004), B-spline and NURBS surfaces are discussed in the literature. We restrict ourselves to this class of surfaces.

There are various ways to approach the fitting problem. The intuitive least squares method for B-splines, which reduces to solving a linear system of equations, depends on finding a valid parameterization and knot vectors, which requires powerful optimization methods (Gálvez et al., 2012). When using NURBS, one also has the possibility to choose the weights, although this is hardly done in practice.

Advanced techniques include iterative methods for B-splines such as applying a Quasi-Newton method for active curves and surfaces (Pottmann et al., 2002), adaptations of iterative geometric interpolation and approximation algorithms (Kineri et al., 2012), iterative approaches for NURBS that avoid solving a linear system at all (Lin et al., 2004), formulations of the fitting problem as more general constrained optimization problems (Flóry, 2009) and hybrid optimization algorithms for NURBS (Xie et al., 2012). Several publications also focus on improving the computational

efficiency, such as (Brujic et al., 2011). Finally we mention that progressive iterative approximation (Deng and Lin, 2014; Delgado and Peña, 2010) is a common technique.

Achieving smoothness across patch interfaces is of primary importance for generating a high-quality geometric model. Approximate methods for the coupling of patches across interfaces are treated e.g. by Shi et al. (2004); Milroy et al. (1995), whereas exact methods are discussed in the recent book of Kiciak (2016).

We consider the spline fitting problem on a single patch including boundary conditions which makes our approach also suitable for generating multi-patch models, in which the boundary conditions may arise from data of neighboring patches. In this context, it is often more important to achieve approximate G^1 smoothness across interfaces between patches than to approximate given point data along interfaces as good as possible. Also, real-world data most likely will contain measurement errors, making it less reasonable to enforce a highly precise fitting result along the interfaces.

Since all patches are considered separately, a geometric model produced by our fitting procedure will be only approximately G^0 (and, in addition to it, approximately G^1) smooth. In certain applications, such as numerical flow simulations, it is desirable to maintain global C^0 smoothness; this can be achieved by simply identifying boundary control points of adjacent patches and solving the fitting problem on all patches simultaneously.

We formulate the problem as an optimization problem, which combines point and normal errors with the use of norm-like functions, thereby generalizing the standard least squares fitting. The paper is organized as follows: In Section 2, we state the problem, introduce the used notation and present our computational approach. Section 3 is devoted to the existence of a series of solutions to the problem described in Section 2 and to analyzing the behavior of their convergence. In Section 4 we present numerical examples both with artificial and industrial data. Section 5 concludes the paper and identifies directions for future work.

2 Simultaneous approximation of point and normal data

Consider the data depicted in Figure 1 (bottom right), which shows a part of a turbine and a turbine blade model. This point cloud is to be approximated by a spline surface. The parameter values shown on top are generated by a standard parameterization method (Floater and Hormann, 2005) for meshes, applied to a triangulation of the data. In order to ensure smooth connections to the neighboring surfaces, we need to enforce approximate G^1 -smoothness by additionally approximating the prescribed normal data along the red boundaries. We do not consider normals along the remaining two boundaries, since the associated neighboring surface patches (blends) are created in a subsequent step.

We realize the fillet surface construction by performing a minimization of the objective function

$$F(s) = \sum_{j=1}^D \nu(|x_s(t_j) - f_j|) + \gamma \sum_{k=1}^K \nu(|Nx_s(\hat{t}_k) - n_k|) \rightarrow \min. \quad (1)$$

In detail,

- $|\cdot|$ denotes the standard Euclidean norm, $\nu : \mathbb{R}^+ \rightarrow \mathbb{R}^+ \in \mathcal{C}^2$ is a *norm-like function*¹ as described by Aigner and Jüttler (2009),
- the approximating spline surface

$$x_s(t) = \sum_{i=1}^n c_i B_i(t), \quad t \in [0, 1]^2,$$

¹In particular, choosing $\nu(x) = x^2$ results in a standard least squares fitting problem. Please note that we consider a more restricted class of norm-like functions than in the original paper, see the assumptions (4) at the end of this section.

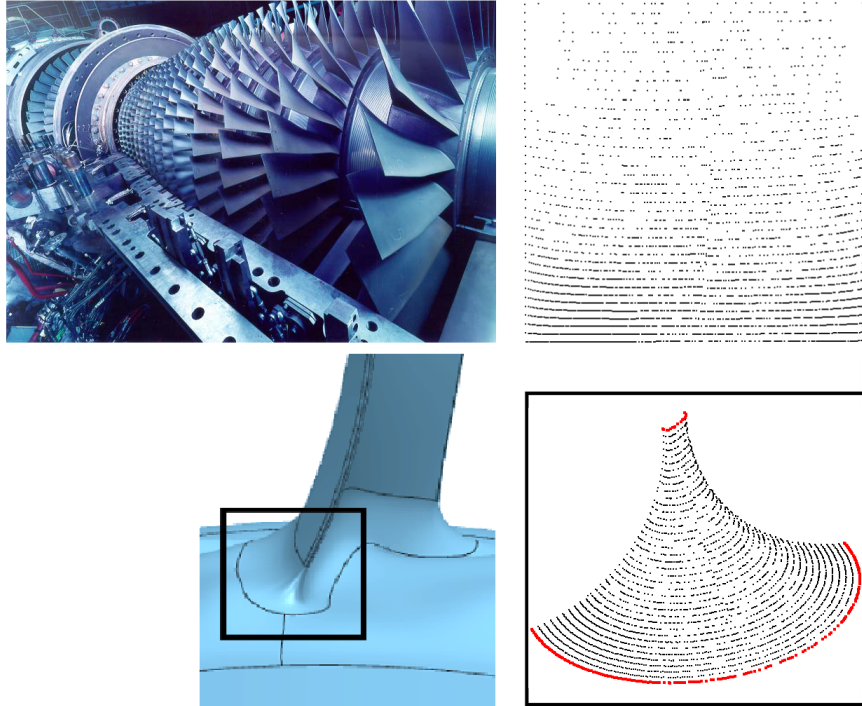


Figure 1: Turbine component (top left) and point cloud: Parametric (top right) and measured physical data (bottom right) of the fillet belonging to the central part of the marked area of the turbine blade (bottom left).

which represents the fillet, depends on the vector

$$s = (c_1^T, \dots, c_n^T) = (c_1^1, c_1^2, c_1^3, c_2^1, \dots, c_n^1, c_n^2, c_n^3)$$

of control points, which are multiplied with either tensor-product B-splines or THB-splines (Kiss et al., 2014) B_i ,

- the surface approximates the given points f_j at parameter values $t_j \in [0, 1]^2$, and the unit normal vectors n_k at parameter values \hat{t}_k ,
- the operator N transforms the surface into the associated field of unit normal vectors, and
- the non-negative weight γ controls the relative influence of points and normals.

In the example shown in Figure 1, the distribution of the parameter values t_j is often quite non-uniform, and the values \hat{t}_k are located on the patch boundary.

Due to the presence of the unit normals and for general norm-like functions, the minimization of (1) leads to a non-linear optimization problem. A necessary condition for s to be a minimizer of (1) is $\nabla F(s) = 0$. We solve this equation approximately by a Gauss-Newton-type method, i.e. a simplified Gauss-Newton method, where in the ℓ -th iteration we solve the linear system

$$H_F(s^\ell) \Delta s = -\nabla F(s^\ell) \quad (2)$$

and update the current solution s^ℓ via $s^{\ell+1} = s^\ell + (\Delta s)^T$. The solution of the standard least squares point fitting problem is used as start value. More precisely, we approximate the Hessian of the objective function by

$$H_F(s) = \sum_{j=1}^D \omega(|R_j|) \nabla R_j^T(s) \nabla R_j(s) + \sum_{k=1}^K \omega(|\hat{R}_k|) \nabla \hat{R}_k^T(s) \nabla \hat{R}_k(s),$$

where $R_j = x_s(t_j) - f_j$ and $\hat{R}_k = Nx_s(\hat{t}_k) - n_k$ are the point and normal residuals, respectively, and

$$\omega(x) = \nu'(x)/x, \quad (3)$$

cf. (Aigner and Jüttler, 2009). The latter function is called the *weight function* associated with the norm-like function ν . The exact computation of the Hessian is costly, therefore the aforementioned approximation is chosen. In (Aigner and Jüttler, 2009) it is shown that in the zero-residual case this expression converges to the true Hessian with respect to the spectral norm.

Besides the obvious choice $\nu(x) = x^2$, it is potentially useful to consider other types of norm-like functions, since they may enhance the performance of the method in the presence of outliers or improve the approximation result. However, for the analysis we restrict ourselves to norm-like functions that satisfy $\nu(0) = 0$ and whose weight functions possess the following properties:

- They have a global lower bound ω_{\min} , i.e., $\omega(x) \geq \omega_{\min}$ holds for all $x \in \mathbb{R}^+$, and
- they possess an upper bound $\omega_{\max}(F)$ on each interval $[0, F]$, i.e., $\omega(x) \leq \omega_{\max}(F)$ holds for all $x \in [0, F]$.

We will refer to these as *norm-like functions with positive and partially bounded weights*. They satisfy

$$\frac{1}{2}\omega_{\min}x^2 \leq \nu(x) \leq \frac{1}{2}\omega_{\max}(F)x^2 \text{ on any interval } [0, F]. \quad (4)$$

It has been shown that in the zero-residual case, the method (2) achieves local quadratic convergence for this class of norm-like functions under certain technical assumptions, see (Aigner and Jüttler, 2009, Theorem 5).

3 Existence of a Solution and Convergence Rates

In order to gain some insight into the behavior of the solution to the minimization problem (1), we consider the continuous version

$$\hat{F}(s) = \|\nu(|x_s - f|)\|_{L^1} + \gamma\|\nu(|Nx_s - Nf|)\|_{L^1} \rightarrow \min, \quad (5)$$

where

$$f : [0, 1]^2 \rightarrow \mathbb{R}^3 \quad (6)$$

is a given smooth surface that we want to approximate. We derived it by replacing the sums with integrals.

It should be noted that the presence of L^1 norms in (5) is caused by the use of the norm-like function ν . In the simplest possible case $\nu(x) = x^2$ one obtains

$$\hat{F}(s) = \|x_s - f\|_{L^2}^2 + \gamma\|Nx_s - Nf\|_{L^2}^2.$$

In this section we restrict the exposition to spline surfaces x_s defined by tensor-product B-splines B_i of degree (p, p) , which are defined over two quasi-uniform open knot vectors $\Xi = (\Xi_1, \Xi_2)$ on $[0, 1]^2$. As usual we use h to denote the mesh size, i.e., the maximum length of the resulting elements.

We recall two basic facts from spline theory:

- Stability of a B-spline basis $\{B_i\}$ (de Boor, 1976, Theorem 4.1; Schumaker, 1981, Theorem 12.5): There exists a constant $0 < D_p \leq 2(p+1)9^p$ such that

$$\frac{1}{D_p^2}|s|_{\infty} \leq \left\| \sum_i c_i B_i \right\|_{L^{\infty}} \leq |s|_{\infty}. \quad (7)$$

These inequalities are valid for splines with scalar coefficients. They can be generalized to spline surfaces by defining

$$\|x_s\|_{L^{\infty}} = \max_{t \in [0, 1]^2} |x_s(t)|$$

and exploiting the equivalence

$$|v|_\infty \leq |v| \leq \sqrt{3}|v|_\infty,$$

of the Euclidean norm $|\cdot|$ and the maximum norm $|\cdot|_\infty$ in \mathbb{R}^3 .

- Approximation power of splines with scalar coefficients (de Boor and Fix, 1973): There exist quasi-interpolation operators Π_Ξ that transform any given function $\phi \in H^{p+1}$ into a spline function $\Pi_\Xi\phi$. More precisely, the error satisfies

$$\|\phi - \Pi_\Xi\phi\|_{L^2} \leq C \cdot h^{p+1} \|\phi\|_{H^{p+1}}, \quad (8)$$

and

$$\|\phi - \Pi_\Xi\phi\|_{H^1} \leq C \cdot h^p \|\phi\|_{H^{p+1}}, \quad (9)$$

where the constant C does not depend on Ξ , h , or f , i.e., points are approximated with order $p+1$, while derivatives are approximated with order p . The result carries over to splines with values in \mathbb{R}^3 by applying Π_Ξ componentwise.

These observations will be used to derive a result about the existence of solutions and the convergence rate as h tends to zero. We consider a regular surface f , see (6), and a norm-like function ν satisfying $\nu(0) = 0$ with positive and bounded weight function, cf. (3) and (4).

Theorem 1. *The problem (5) has a solution for all pairs Ξ of knot vectors. The sequence of solutions realizes the optimal approximation order if $\gamma = \gamma_0 h^2$ for some positive constant γ_0 .*

Before proving Theorem 1 we state an auxiliary result.

Lemma 2. *There exists constants $C_N = C_N(f)$ and $h_0 = h_0(f)$, which depend on the given surface f , such that*

$$\|N\Pi_\Xi f - Nf\|_{L^2} \leq C_N h^p$$

holds whenever $h < h_0$, where $\Pi_\Xi f$ is applied to the elements of f , i.e.

$$\Pi_\Xi f = \begin{pmatrix} \Pi_\Xi f^1 \\ \Pi_\Xi f^2 \\ \Pi_\Xi f^3 \end{pmatrix}.$$

The proof of this Lemma 2 follows from the approximation order of the derivatives and the fact that the normal depends continuously on the derivatives, taking the regularity of the parameterization into account. We present the details of this proof in the appendix.

Proof of Theorem 1. First, we show that a solution exists for any pair of knot vectors. We restrict the $\|\cdot\|_{L^\infty}$ - and the $\|\cdot\|_{L^2}$ -norm to the spline space $\text{span}\{B_i | i \in I_h\}$ which has finite dimension. Consequently, the two norms are equivalent, i.e., there exists a constant C_{norm} such that

$$\left\| \sum_{i \in I_h} c_i B_i \right\|_{L^\infty} \leq C_{\text{norm}} \left\| \sum_{i \in I_h} c_i B_i \right\|_{L^2}. \quad (10)$$

We combine this observation with (7) and obtain

$$\frac{1}{C_{\text{norm}}} \frac{1}{D_p^2} |s^*|_\infty \leq \|x_{s^*}\|_{L^2} = \|x_{s^*} - f + f\|_{L^2},$$

where s^* is the solution of (5). Now using the triangle inequality, the first inequality in (4) and the identity

$$\|\cdot\|_{L^2} = \sqrt{\|(\cdot)^2\|_{L^1}}$$

gives

$$\frac{1}{C_{\text{norm}}} \frac{1}{D_p^2} |s^*|_\infty \leq \sqrt{\frac{2}{\omega_{\min}} \|\nu(|x_{s^*} - f|)\|_{L^1} + \|f\|_{L^2}}. \quad (11)$$

The L^1 norm on the right-hand side is bounded by $\hat{F}(s)$ for any choice of s . In particular we may choose s as null vector and obtain

$$\frac{1}{C_{\text{norm}}} \frac{1}{D_p^2} |s^*|_{\infty} \leq \sqrt{\frac{2}{\omega_{\min}} (\|\nu(|f|)\|_{L^1} + \gamma \|\nu(|Nf|)\|_{L^1}) + \|f\|_{L^2}}. \quad (12)$$

Consequently, it suffices to consider the objective function (5) on the closed ball with radius

$$C_{\text{norm}} D_p^2 \left(\sqrt{\frac{2}{\omega_{\min}} (\|\nu(|f|)\|_{L^1} + \gamma \|\nu(|Nf|)\|_{L^1}) + \|f\|_{L^2}} \right),$$

which is a compact domain. The continuity of the objective function thus ensures the existence of the minimum.

In order to establish the optimality of the approximation order, we consider a sequence of knot pairs $\Xi = \Xi_h$ with decreasing element size h and show that the point and normal errors of the solutions to (5) satisfy

$$\sqrt{\|\nu(|x_h - f|)\|_{L^1}} \leq C' h^{p+1} \quad \text{and} \quad \sqrt{\|\nu(|Nx_h - Nf|)\|_{L^1}} \leq C' h^p \quad (13)$$

for some constant C' , which is independent of h .

As

$$\|\Pi_{\Xi} f - f\|_{L^{\infty}([0,1]^2)}$$

is bounded and since

$$|(\Pi_{\Xi} f - f)(t)| \leq \|\Pi_{\Xi} f - f\|_{L^{\infty}([0,1]^2)} \quad \text{for almost all } t \in [0, 1]^2$$

we choose

$$F = \max\{2, \|\Pi_{\Xi} f - f\|_{L^{\infty}([0,1]^2)}\}$$

and obtain

$$\begin{aligned} & \|\nu(|\Pi_{\Xi} f - f|)\|_{L^1} + \gamma_0 h^2 \|\nu(|N\Pi_{\Xi} f - Nf|)\|_{L^1} \\ & \leq \left\| \sqrt{\frac{\omega_{\max}(F)}{2}} |\Pi_{\Xi} f - f| \right\|_{L^2}^2 + \gamma_0 h^2 \left\| \sqrt{\frac{\omega_{\max}(F)}{2}} |N\Pi_{\Xi} f - Nf| \right\|_{L^2}^2. \end{aligned}$$

Thus, the value of objective function at the coefficients of the surfaces $\Pi_{\Xi} f$ has the upper bound

$$\frac{\omega_{\max}(F)}{2} (C^2 + \gamma_0 C_N^2) h^{2p+2},$$

where the constants C and C_N are taken from (8) and Lemma 2, respectively. This implies that the solution of (5) satisfies (13) with

$$C' = \max \left\{ \sqrt{\frac{\omega_{\max}(F)}{2} (C^2 + \gamma_0 C_N^2)}, \sqrt{\frac{\omega_{\max}(F)}{2} \frac{C^2 + \gamma_0 C_N^2}{\gamma_0}} \right\}.$$

□

This result is equivalent to the simple observation that – under a suitable regularity assumption – the unit normals possess the same approximation order as the derivatives. It carries over to the considered class of norm-like functions, which satisfy (4) and $\nu(0) = 0$.

It should be noted that the choice of γ , which is described in the above theorem, is similar to the weights that appear in the jump and average terms used in the discontinuous Galerkin discretization of partial differential equations, cf. Seiler and Jüttler (2017).

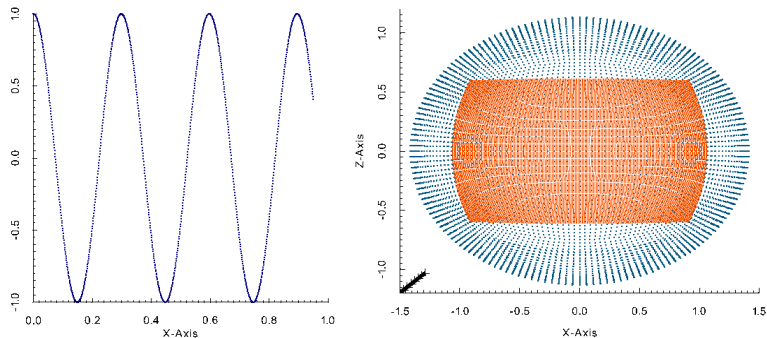


Figure 2: One- (left) and two-dimensional (right) synthetic data for the numerical tests.

4 Numerical Experiments

This section has three parts. First, we verify the theoretical results of the previous section by considering synthetic data sets. Second, we apply the fitting technique to the industrial data set representing the fillet surface. Finally, we explore the effects of using norm-like functions.

4.1 Least-squares fitting: Synthetic data

We demonstrate the theoretical findings concerning the convergence rates by applying the fitting procedure with the trivial norm-like function $\nu(x) = x^2$ to two synthetic data sets. First, we generated point and normal data by uniformly sampling 10^4 points and normals from the graph of the trigonometric curve $\cos(20t)$, $t \in [0, 1]$. Second we consider another data set obtained by evaluating 201^2 points and normals on a uniform grid in the domain of the ellipsoidal patch

$$(t_1, t_2) \mapsto \begin{pmatrix} \frac{3}{2} \cdot \cos(\frac{\pi}{3}t_1 - \frac{\pi}{6}) \cdot \cos(\frac{\pi}{2}t_2 + \frac{5\pi}{4}) \\ \frac{4}{5} \cdot \cos(\frac{\pi}{3}t_1 - \frac{\pi}{6}) \cdot \sin(\frac{\pi}{2}t_2 + \frac{5\pi}{4}) \\ \frac{6}{5} \cdot \sin(\frac{\pi}{3}t_1 - \frac{\pi}{6}) \end{pmatrix}, \quad t \in [0, 1]^2, \quad (14)$$

see Figure 2, highlighted patch.

We computed the approximation result by using Gauss-Newton method described in Section 2. The iterative procedure was terminated when the gradient of the objective function satisfied $|\nabla F(s^\ell)| \leq 10^{-8}$ or when the iteration count reached 500 (but this was never the case for the two synthetic data sets). The basis functions B_i were chosen as (bi-) cubic (tensor-product) B-splines. We consider uniform open knot vectors with mesh size h varying between 1 and 2^{-8} or 2^{-5} for curves and surfaces, respectively.

Figures 3 and 4 report the resulting sum of squared errors with respect to the Euclidean norm for $\gamma = h^k$, $k = 0, 1, 2, 3$ and for $\gamma = 0$. Among the considered choices of the weight γ , the optimal rates of convergence (4 for the point data and simultaneously 3 for the normals) are achieved for $\gamma = h^2$, $\gamma = h^3$ and for $\gamma = 0$. The first case is covered by the theoretical results in the previous section, while the other ones confirm that standard L^2 approximation also provides the optimal rate of convergence of the derivatives. Consequently, using the normal vectors does not provide any advantages for synthetic data. However, the example in the next section will demonstrate the benefits for an industrial application.

Figures 5 and 6 demonstrate the influence of the constant γ_0 . It can be seen that the fitting result is fairly robust with respect to variations of this weight. Note that the effects of changing γ_0 are not invariant under scaling. This issue can be resolved by performing a suitable scaling of the data.

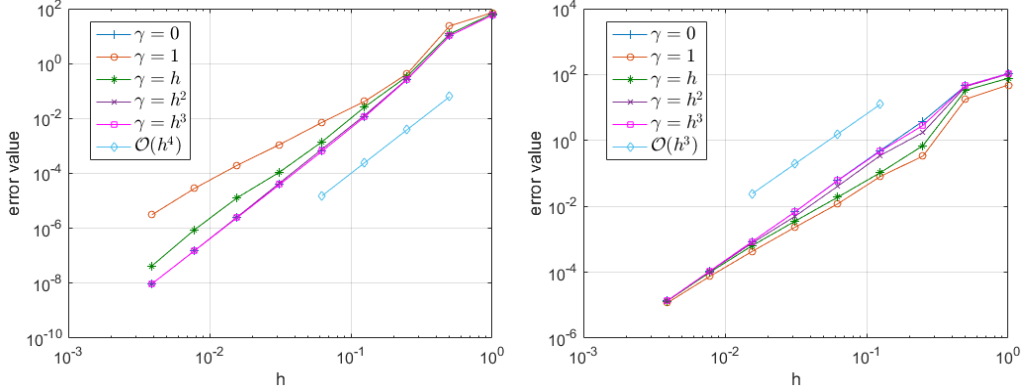


Figure 3: Synthetic curve data: Point (left) and normal (right) error for various choices of weight γ and mesh size h .

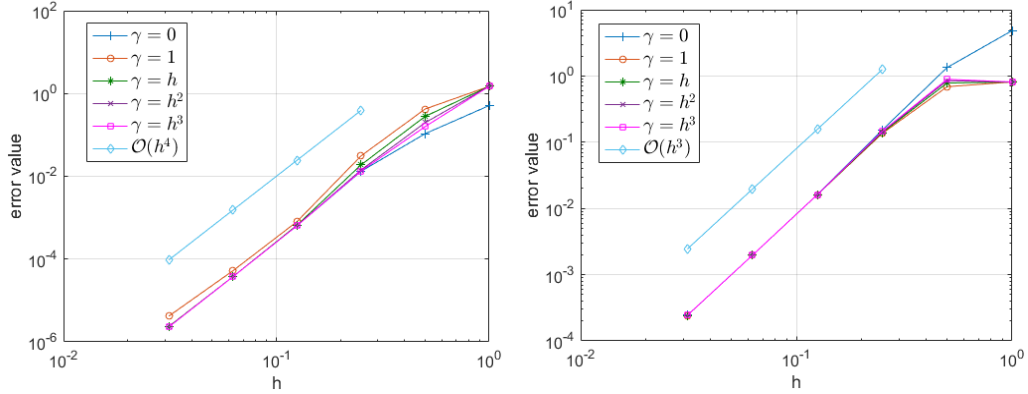


Figure 4: Synthetic surface data: Point (left) and normal (right) error for various choices of weight γ and mesh size h .

4.2 Least-squares fitting: Industrial data

Next we apply the fitting procedure to the fillet data shown in Figure 1, which consists of 3280 point and 214 normal samples. The normal data is available only at top and bottom of the fillet, in order to ensure a smooth connection to the adjacent patches. First we consider tensor-product discretizations with varying mesh size h (up to 1225 control points) obtained by dyadic refinement. We regularized the objective function by introducing a quadratic surface energy with weight $\lambda = 10^{-5}$, see Kiss et al. (2014) for details. This also has a fairing effect.

Figure 7, light and dark blue curves, visualizes the resulting sum of squared errors with respect to the Euclidean norm for $\gamma = 10^{-3}h^2$ and for $\gamma = 0$ (without normals). It can be seen that using the normal data is essential, since the normals do not converge for $\gamma = 0$. Clearly, one cannot expect to achieve the same convergence rate as for the synthetic data, due to measurement errors. Also, the normals were sampled from neighboring patches, not from the fillet.

Figure 8 depicts the resulting fillet patches with (right) and without (left) approximating normal vectors for the finest tensor-product spline discretization. We added reflection lines to visualize the surface quality. On the one hand, the use of normal data (right) clearly improves the G^1 smoothness across the patch boundaries, since the reflection lines are continuous. This is especially visible in the marked areas, which are shown again in Figure 9, where there are discontinuities in the reflection lines of the left plot and smoother transitions in the reflection lines of the right plot. However, even at the finest discretization with 1225 control points, the normal error was still relatively large (sum of squared errors $6.1 \cdot 10^{-7}$ and maximum angle $1.65 \cdot 10^{-2}$ degrees for $\gamma = 10^{-3}h^2$).

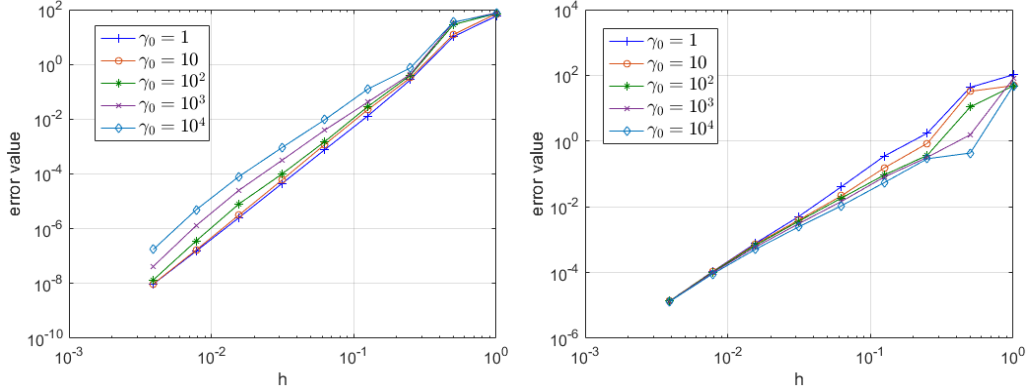


Figure 5: Synthetic curve data: Point (left) and normal (right) error for various choices of the constant γ_0 where $\gamma = \gamma_0 h^2$.

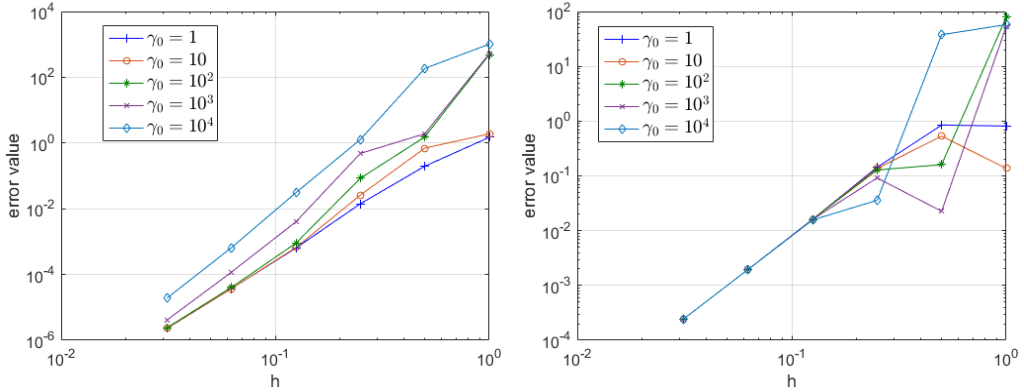


Figure 6: Synthetic surface data: Point (left) and normal (right) error for various choices of the constant γ_0 where $\gamma = \gamma_0 h^2$.

A further improvement – even when using a much smaller number of degrees of freedom – can be obtained by employing THB-spline discretizations instead of tensor-product splines, similar to the techniques reported by Kiss et al. (2014); Giannelli et al. (2016). We use the absolute threshold refinement strategy with $\varepsilon = 10^{-6}$ and compare the results obtained without (left) and with (right) using normal data in Figure 10. Both surfaces have acceptable quality, but the use of normal data again improves the G^1 smoothness (see close-up views). The leftmost reflection line is discontinuous without normal information.

Table 1 reports the resulting errors for the two THB-spline approximations. In particular, while the use of normal data does not compromise the point error, it significantly improves the approximate G^1 smoothness. Here, h refers to the mesh size of the finest discretization level.

The finest THB-spline discretization with 841 control points leads to a significantly smaller normal error than the finest uniform discretization (sum of squared errors norm $2.01 \cdot 10^{-8}$ and maximum angle $3.24 \cdot 10^{-3}$ degrees for $\gamma = 10^{-3} h^2$).

The sum of squared errors with respect to the Euclidean norm for $\gamma = 10^{-3} h^2$ and for $\gamma = 0$ (without normals) for different numbers of control points is shown in Figure 7, dark and light red curves. Here, again, the effect of reaching a smaller normal error with less control points is evident.

Clearly, we obtain different THB meshes for $\gamma = 0$ and $\gamma = 10^{-3} h^2$, which are visualized in Figure 11. The two surfaces have 556 and 841 control points. The use of the normal data led to additional refinement near the boundaries.

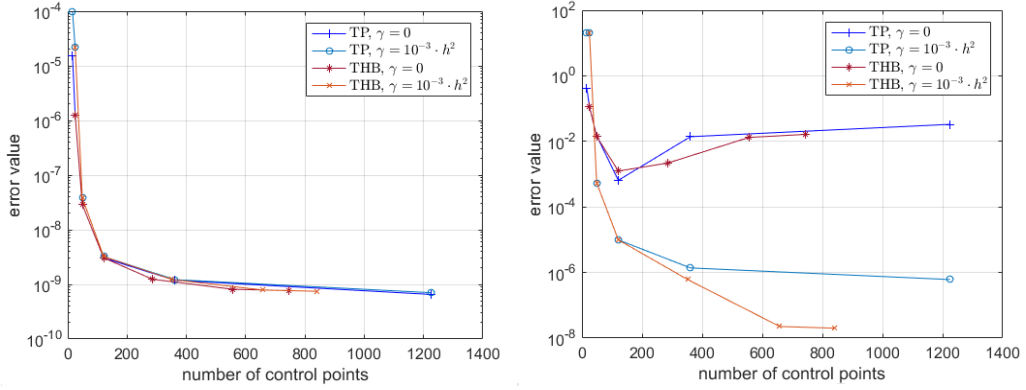


Figure 7: Point (left) and normal (right) error for tensor-product (blue) and THB-spline (red) approximations of the fillet data.

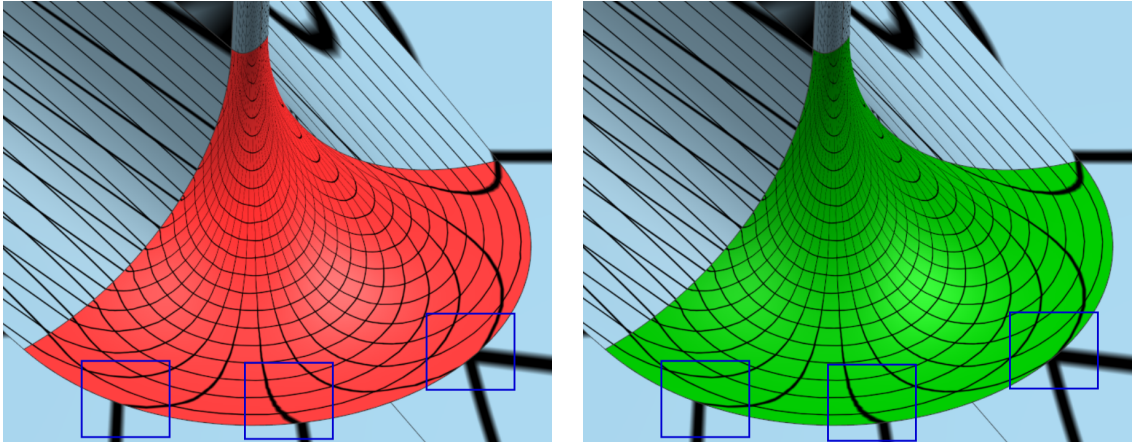


Figure 8: Tensor-product spline approximations of the fillet data without (left) and with (right) using normal information.

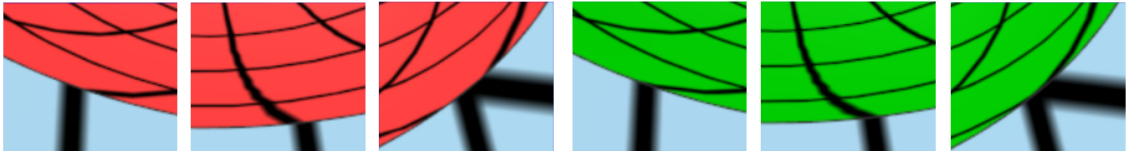


Figure 9: The details shown in the marked areas from left to right.

4.3 Norm-like functions

Now we consider the influence of different choices of ν while neglecting the normal data approximation term, using the data previously introduced (Figure 1 and 2, right). We artificially introduce outliers to the ellipsoidal patch values in order to illustrate the effects of different alternatives of ν . More precisely, we set the value of the third component of three of the 201^2 samples to 1.5 instead of 1.02083, 1.02901 and 0.979487, respectively. Thus, the outliers have a distance of 0.64977, 0.65063 and 0.67656 from the original data points. We do not have further information about the industrial data from Figure 1, but most likely there will be some noise in the data.

Following Aigner and Jüttler (2009), we select the norm-like functions

- $\nu_1(x) = 1 - \exp(-\eta^2 x^2)$,
- $\nu_2(x) = x^2$, which corresponds to a standard least-squares fitting problem, and
- $\nu_3(x) = \exp(\eta^2 x^2) - 1$.

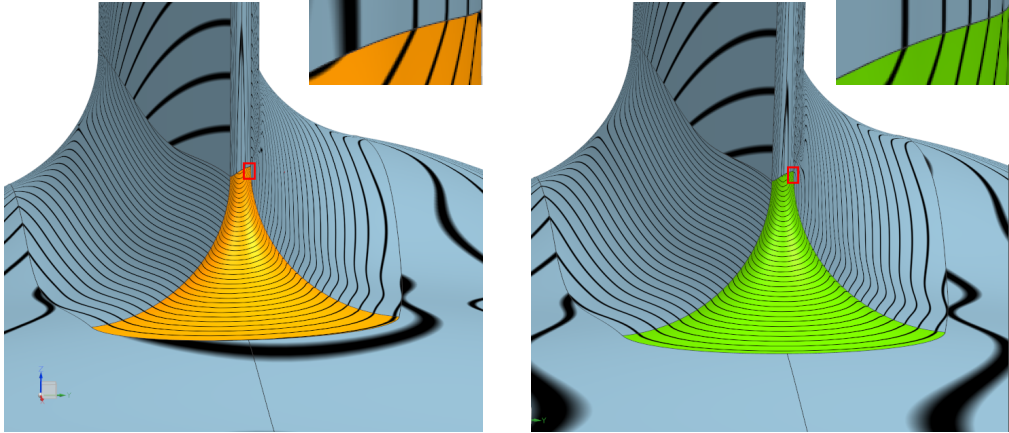


Figure 10: Top: THB-spline approximations of the fillet data without (left) and with (right) using normal information.

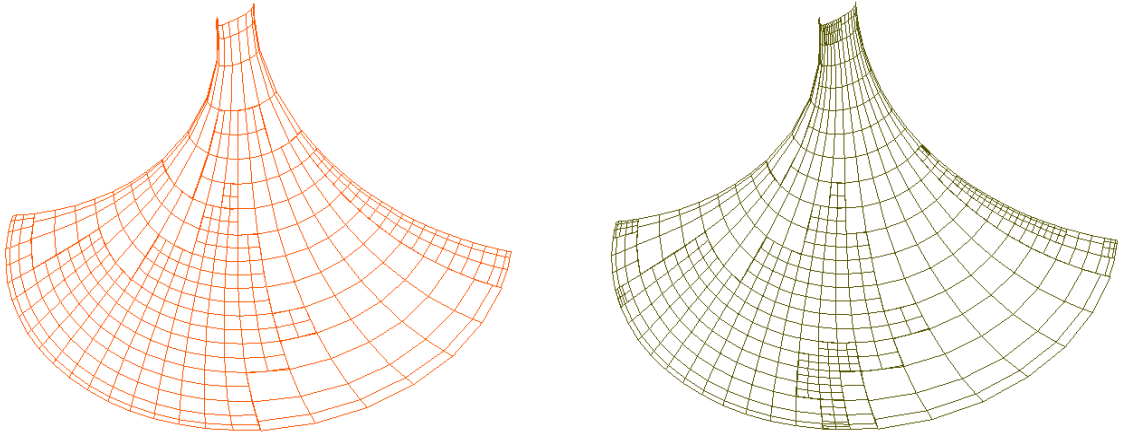


Figure 11: Control nets of the THB-spline surfaces approximating the fillet data without (left) and with (right) using normal information.

The constant η was chosen as described in Aigner and Jüttler (2009). Minimizing the first and the third function, which are motivated by the statistics literature, has been observed to have a beneficial effect on outliers and on the maximum error, respectively.

The latter two functions are norm-like functions with positive and partially bounded weights, since they fulfill the assumptions specified in Section 2. In contrast, the weight function associated with $\nu_1(x)$ is not globally bounded from below. One may replace the weight by a constant for all arguments exceeding some threshold, in order to satisfy the assumptions.

For the results in Table 2 we used a tensor-product B-spline discretization with B-splines of degree (3,3) and mesh size $h = 0.03125$, as in the previous experiments, and we set $\gamma = 0$. As expected the ℓ_1 -error is minimal when using ν_1 and an analogous outcome is visible for the other two norms. Note that the differences between the error values are more distinct for the ellipsoidal patch data than for the fillet data set which is due to the presence of very few strong outliers. The influence of the choice of ν is not visible for the fillet data where the error appears to have a more uniform distribution.

5 Conclusion

We considered the simultaneous approximation of point and normal data using norm-like functions. This leads to a non-linear optimization problem, which has been solved by a Gauss-Newton-type

	without normals	with normals
	$\gamma = 0, 3 \times 556$ dofs	$\gamma = 10^{-3}h^2, 3 \times 841$ dofs
$\sum_j \ x_{s,h}(t_j) - f_j\ _2^2$	$8.15 \cdot 10^{-10}$	$7.48 \cdot 10^{-10}$
$\sum_k \ Nx_{s,h}(t_k) - n_k\ _2^2$	$1.32 \cdot 10^{-2}$	$2.01 \cdot 10^{-8}$
maximum angle between normals in degree	0.94	$3.24 \cdot 10^{-3}$

Table 1: Error values of the THB-spline approximations.

	Ellipsoid data with outliers			Fillet data		
	$\nu_1(x)$	$\nu_2(x)$	$\nu_3(x)$	$\nu_1(x)$	$\nu_2(x)$	$\nu_3(x)$
$\sum_j \ R_j\ _2$	6.1	7.17	7.86	0.001242	0.001242	0.001248
$\sqrt{\sum_j \ R_j\ _2^2}$	1.1	1.0942	1.095	$2.42 \cdot 10^{-5}$	$2.42 \cdot 10^{-5}$	$2.43 \cdot 10^{-5}$
$\max_j \ R_j\ _2$	0.66	0.65	0.64	$1.514 \cdot 10^{-6}$	$1.514 \cdot 10^{-6}$	$1.513 \cdot 10^{-6}$

Table 2: Error values in different ℓ_p norms for approximations of the ellipsoidal patch and fillet data.

technique, based on the earlier results reported by Aigner and Jüttler (2009). We used an industrial data set to illustrate the advantages of fitting point and normal data simultaneously. In this context we combined our approach with the mathematical technology of truncated hierarchical B-splines (THB-splines), which provided again a significant improvement of the fitting results. As observed in our experiments, the use of normal information helps greatly to maintain approximate G^1 smoothness across patch boundaries.

In our future research we plan to explore applications in isogeometric analysis, in particular concerning isogeometric multi-patch discretizations possessing approximate geometric smoothness. So far, the construction of smooth multi-patch discretizations in isogeometric analysis (which is of vital interest, e.g., when considering high-order problems) is almost exclusively based on the notion of exact geometric continuity, see e.g. Kapl et al. (2015); Groisser and Peters (2015); Kapl et al. (2018). Approximate methods may help to overcome the resulting limitations of approximation power and geometric flexibility, and this motivates us to investigate them further.

A further improvement of the fitting results could be achieved by performing an optimization of the parameters also, using methods such as parameter correction (Hoschek, 1988). This is beyond the scope of the present paper. Last, but not least, it might be possible to generalize the observations made in Section 3 to hierarchical splines, based on the recent results of Speleers and Manni (2016) on quasi-interpolation operators for THB-splines.

Appendix: Proof of Lemma 2.

For $p > \frac{3}{2}$ and for sufficiently small element size, the derivatives of given surface f and of its spline approximation $\Pi_{\Xi}f$ satisfy

$$\|\partial_1 f\|_{L^\infty} \leq M, \quad \|\partial_2 f\|_{L^\infty} \leq M, \quad (15)$$

$$\|\partial_1 \Pi_{\Xi} f\|_{L^\infty} \leq M, \quad \|\partial_2 \Pi_{\Xi} f\|_{L^\infty} \leq M, \quad (16)$$

$$|\partial_1 f(t) \times \partial_2 f(t)| \geq m, \quad |\partial_1 \Pi_{\Xi} f(t) \times \partial_2 \Pi_{\Xi} f(t)| \geq m \quad \forall t \in [0, 1]^2 \quad (17)$$

for some constants $M, m > 0$ (see Adams and Fournier, 2003). Note that the latter two inequalities are induced by the regularity assumption for the surface f .

We consider the difference of the unit normals,

$$\left\| \frac{\partial_1 f \times \partial_2 f}{|\partial_1 f \times \partial_2 f|} - \frac{\partial_1 \Pi_{\Xi} f \times \partial_2 \Pi_{\Xi} f}{|\partial_1 \Pi_{\Xi} f \times \partial_2 \Pi_{\Xi} f|} \right\|_{L^2}. \quad (18)$$

The subtrahend of the difference can be rewritten as

$$\frac{\left(\frac{|\partial_1 \Pi_{\Xi} f \times \partial_2 \Pi_{\Xi} f|^2}{|\partial_1 f \times \partial_2 f|} \partial_1 f + |\partial_1 \Pi_{\Xi} f \times \partial_2 \Pi_{\Xi} f| \partial_1 \Pi_{\Xi} f - \frac{|\partial_1 \Pi_{\Xi} f \times \partial_2 \Pi_{\Xi} f|^2}{|\partial_1 f \times \partial_2 f|} \partial_1 f \right) \times (\partial_2 f + \partial_2 \Pi_{\Xi} f - \partial_2 f)}{|\partial_1 \Pi_{\Xi} f \times \partial_2 \Pi_{\Xi} f|^2}$$

After substituting the rewritten subtrahend into (18), we expand the cross product and use the triangle inequality to expand the result into four terms.

The first term

$$\left\| \frac{\partial_1 f \times \partial_2 f}{|\partial_1 f \times \partial_2 f|} - \frac{\partial_1 f \times \partial_2 f}{|\partial_1 f \times \partial_2 f|} \right\|_{L^2}$$

is equal to zero. The second term satisfies

$$\left\| \frac{1}{|\partial_1 f \times \partial_2 f|} (\partial_1 f \times (\partial_2 \Pi_{\Xi} f - \partial_2 f)) \right\|_{L^2} \leq \frac{1}{m} \cdot M \cdot C \cdot h^p \cdot \|f\|_{H^{p+1}}.$$

The third term takes the form

$$\left\| \frac{(|\partial_1 \Pi_{\Xi} f \times \partial_2 \Pi_{\Xi} f| |\partial_1 f \times \partial_2 f| |\partial_1 \Pi_{\Xi} f - |\partial_1 \Pi_{\Xi} f \times \partial_2 \Pi_{\Xi} f|^2 \partial_1 f) \times \partial_2 f}{|\partial_1 \Pi_{\Xi} f \times \partial_2 \Pi_{\Xi} f|^2 |\partial_1 f \times \partial_2 f|} \right\|_{L^2}.$$

The first factor of the numerator can be rewritten as

$$\begin{aligned} & |\partial_1 \Pi_{\Xi} f \times \partial_2 \Pi_{\Xi} f| \cdot |\partial_1 f \times \partial_2 f| |\partial_1 \Pi_{\Xi} f - |\partial_1 \Pi_{\Xi} f \times \partial_2 \Pi_{\Xi} f|^2 \partial_1 f \\ & + |\partial_1 \Pi_{\Xi} f \times \partial_2 \Pi_{\Xi} f| \cdot |\partial_1 f \times \partial_2 f| |\partial_1 f - |\partial_1 \Pi_{\Xi} f \times \partial_2 \Pi_{\Xi} f| \cdot |\partial_1 f \times \partial_2 f| \partial_1 f. \end{aligned}$$

This helps us to obtain an upper bound for the third term,

$$\frac{M}{m} \|\partial_1 \Pi_{\Xi} f - \partial_1 f\|_{L^2} + \frac{M^2}{m^2} \|(\partial_1 f \times \partial_2 f) - (\partial_1 \Pi_{\Xi} f \times \partial_2 \Pi_{\Xi} f)\|_{L^2}.$$

Using the properties (9) of the spline projector confirms that this can be bounded by

$$\frac{M}{m} C \cdot h^p \cdot \|f\|_{H^{p+1}} + 4 \frac{M^2}{m} C \cdot h^p \cdot \|f\|_{H^{p+1}},$$

where we used the observation that

$$\begin{aligned} & \|(\partial_1 f \times \partial_2 f) - (\partial_1 \Pi_{\Xi} f - \partial_2 \Pi_{\Xi} f)\|_{L^2} \\ & = \|(\partial_1 f \times \partial_2 f) - ((\partial_1 f + \partial_1 \Pi_{\Xi} f - \partial_1 f) \times (\partial_2 f + \partial_2 \Pi_{\Xi} f - \partial_2 f))\|_{L^2} \\ & = \|(\partial_1 f \times \partial_2 f) - (\partial_1 f \times \partial_2 f) - ((\partial_1 \Pi_{\Xi} f - \partial_1 f) \times \partial_2 f) \\ & \quad - (\partial_1 f \times (\partial_2 \Pi_{\Xi} f - \partial_2 f)) - ((\partial_1 \Pi_{\Xi} f - \partial_1 f) \times (\partial_2 \Pi_{\Xi} f - \partial_2 f))\|_{L^2} \\ & \leq M \|\partial_1 \Pi_{\Xi} f - \partial_1 f\|_{L^2} + M \|\partial_2 \Pi_{\Xi} f - \partial_2 f\|_{L^2} + 2M \|\partial_2 \Pi_{\Xi} f - \partial_2 f\|_{L^2}. \end{aligned}$$

Finally, the expansion generates a fourth term, which is equal to

$$\left\| \frac{\left(|\partial_1 \Pi_{\Xi} f \times \partial_2 \Pi_{\Xi} f| |\partial_1 \Pi_{\Xi} f - \frac{|\partial_1 \Pi_{\Xi} f \times \partial_2 \Pi_{\Xi} f|^2}{|\partial_1 f \times \partial_2 f|} \partial_1 f \right) \times (\partial_2 \Pi_{\Xi} f - \partial_2 f)}{|\partial_1 \Pi_{\Xi} f \times \partial_2 \Pi_{\Xi} f|^2} \right\|_{L^2}$$

and can be dealt with in the same way as for the third one.

Summing up, all four terms are bounded by terms of the form $\frac{1}{4} C_N h^p$ for a suitable choice of the constant C_N (which depends on f). This completes the proof.

Acknowledgment

The authors are indebted to the reviewers for their constructive comments, which have led to a significant improvement of the paper. They were supported by the project EXAMPLE (GA no. 324340) and the Austrian Science Fund (FWF) through the DK W1214-04.

References

- Adams, R., Fournier, J., 2003. Sobolev Spaces. 2nd edition. Pure and Applied Mathematics, Elsevier/Academic Press, Amsterdam.
- Aigner, M., Jüttler, B., 2009. Distance regression by Gauss-Newton-type methods and iteratively re-weighted least-squares. *Computing* 86, 73–87.
- de Boor, C., 1976. On local linear functionals that vanish at all B-splines but one, in: Law, A., Sahney, B. (Eds.), *Theory of Approximation with Applications*, Academic Press, New York. pp. 120–145.
- de Boor, C., Fix, G., 1973. Spline approximation by quasiinterpolants. *Journal of Approximation Theory* 8, 19–45.
- Brujic, D., Ainsworth, I., Ristic, M., 2011. Fast and accurate NURBS fitting for reverse engineering. *International Journal of Advanced Manufacturing Technology* 54, 691–700.
- Delgado, J., Peña, J.M., 2010. A comparison of different progressive iteration approximation methods, in: Dæhlen, M., et al. (Eds.), *Mathematical Methods for Curves and Surfaces*, Springer, Berlin. pp. 136–152.
- Deng, C., Lin, H., 2014. Progressive and iterative approximation for least squares B-spline curve and surface fitting. *CAD Computer Aided Design* 47, 32–44.
- Dierckx, P., 1995. *Curve and Surface Fitting with Splines*. Monographs on Numerical Analysis, Oxford Science Publications.
- Floater, M., Hormann, K., 2005. Surface parameterization: a tutorial and survey, in: *Advances in Multiresolution for Geometric Modelling*, Springer, Berlin. pp. 157–186.
- Flöry, S., 2009. Fitting curves and surfaces to point clouds in the presence of obstacles. *Computer Aided Geometric Design* 26, 192–202.
- Gálvez, A., Iglesias, A., Puig-Pey, J., 2012. Iterative two-step genetic-algorithm-based method for efficient polynomial B-spline surface reconstruction. *Information Sciences* 182, 56–76.
- Giannelli, C., et al., 2016. THB-splines: An effective mathematical technology for adaptive refinement in geometric design and isogeometric analysis. *Comp. Meth. Appl. Mech. Engrg.* 299, 337–365.
- Groisser, D., Peters, J., 2015. Matched G^k -constructions always yield C^k -continuous isogeometric elements. *Computer Aided Design* 34, 67–72.
- Hansford, D., Farin, G., 2002. Curve and surface reconstruction, in: Farin, G., Hoschek, J., Kim, M.S. (Eds.), *Handbook of Computer Aided Geometric Design*. Elsevier. chapter 7, pp. 165–192.
- Hoschek, J., 1988. Intrinsic parametrization for approximation. *Computer Aided Geometric Design* 5, 27–31.
- Jüttler, B., Felis, A., 2002. Least-squares fitting of algebraic spline surfaces. *Advances in Computational Mathematics* 17, 135–152.
- Kapl, M., Sangalli, G., Takacs, T., 2018. Construction of analysis-suitable G^1 planar multi-patch parameterizations. *Computer-Aided Design* 97, 41–55.
- Kapl, M., Vitrih, V., Jüttler, B., Birner, K., 2015. Isogeometric analysis with geometrically continuous functions on two-patch geometries. *Comput. Math. Appl.* 70, 1518–1538.
- Kiciak, P., 2016. Geometric continuity of curves and surfaces. *Synthesis Lectures on Visual Computing* 8, 1–249.

- Kineri, Y., Wang, M., Lin, H., Maekawa, T., 2012. B-spline surface fitting by iterative geometric interpolation/approximation algorithms. *CAD Computer Aided Design* 44, 697–708.
- Kiss, G., et al., 2014. Adaptive CAD model (re-)construction with THB-splines. *Graphical Models* 76, 273–288.
- Lin, H., Wang, G., Dong, C., 2004. Constructing iterative non-uniform B-spline curve and surface to fit data points. *Science in China, Series F: Information Sciences* 47, 315–331.
- Ma, W., 2005. Subdivision surfaces for CAD - an overview. *CAD Computer Aided Design* 37, 693–709.
- Marinov, M., Kobbelt, L., 2005. Optimization methods for scattered data approximation with subdivision surfaces. *Graphical Models* 67, 452–473.
- Milroy, M., Bradley, C., Vickera, G., Weir, D., 1995. G^1 continuity of B-spline surface patches in reverse engineering. *Computer-Aided Design* 27, 471–478.
- Pottmann, H., Leopoldseder, S., Hofer, M., 2002. Approximation with active B-spline curves and surfaces, in: *Proceedings of the 10th Pacific Conference on Computer Graphics and Applications*, IEEE Computer Society, Washington, DC, USA. pp. 8–25.
- Schumaker, L.L., 1981. *Spline Functions: Basic Theory*. Wiley, New York.
- Seiler, A., Jüttler, B., 2017. Reparameterization and adaptive quadrature for the isogeometric discontinuous Galerkin method, in: Floater, M., et al. (Eds.), *Mathematical Methods for Curves and Surfaces*, Springer. pp. 251–269.
- Shi, X., Wang, T., Wu, P., Liu, F., 2004. Reconstruction of convergent G^1 smooth B-spline surfaces. *Computer Aided Geometric Design* 21, 893–913.
- Speleers, H., Manni, C., 2016. Effortless quasi-interpolation in hierarchical spaces. *Numerische Mathematik* 132, 155–184.
- Varady, T., 1997. Reverse engineering of geometric models - an introduction. *Computer-aided design* 29, 255–268.
- Xie, W.C., Zou, X.F., Yang, J.D., Yang, J.B., 2012. Iteration and optimization scheme for the reconstruction of 3D surfaces based on non-uniform rational B-splines. *CAD Computer Aided Design* 44, 1127–1140.